



# Continuous and discontinuous stability analysis of the bell-shaped caverns at Bet Guvrin, Israel

Y.H. Hatzor<sup>a,\*</sup>, M. Talesnick<sup>b</sup>, M. Tsesarsky<sup>a</sup>

<sup>a</sup>Department of Geological and Environmental Sciences, Ben-Gurion University of the Negev, Beer-Sheva 84105, Israel

<sup>b</sup>Department of Geotechnology, Faculty of Civil Engineering, The Technion, Haifa, Israel

Accepted 3 June 2002

## Abstract

The stability of two systems of bell-shaped caverns excavated some 1000 years ago at Bet Guvrin National Park is investigated. The caverns were excavated in a weak, anisotropic, and moderately discontinuous chalk. The cavern stability is considered based on two separate and independent methods: a continuum model framework—FLAC, used for stress analysis, and a discontinuous approach—block theory, used for critical key block analysis.

The numerical stress analysis reveals that in the case of very large span openings, tensile fracture of intact rock may be responsible for instabilities, which may lead to global failure. Evidence of tensile rupture at margins of failed caverns is abundant at the Park.

The discontinuous block theory analysis reveals that the moderate joint set spacing at Bet Guvrin, up to 45% of the roof area may be comprised of removable blocks. The removable keyblocks in the roof remain in place due to arching stresses, which develop through the roof material. The chalk at the roof can sustain the maximum loads in existing caverns, as predicted by the numerical stress analysis. However, local failures due to exceedingly high compressive stresses at the abutments or by tensile fracture at the roof, may lead to relaxation of arching stresses followed by keyblock displacement. Such a “mixed failure mode” process could eventually lead, over time, to global collapse. Indications that “mixed failure mode” processes are presently active in the studied caverns are substantiated by in-situ measurement of keyblock displacements.

It is suggested that in weak and discontinuous rock environments where “mixed failure mode” processes may be active, long term stability evaluation should be based on both continuous and discontinuous stability analyses.

© 2002 Elsevier Science Ltd. All rights reserved.

*Keywords:* Tunneling; Ancient caverns; Chalk; Strength; Anisotropy; Stress distribution; FLAC; Block theory; Critical keyblock; Monitoring

## 1. Introduction

### 1.1. The ancient bell-shaped caverns at Bet Guvrin

The bell-shaped caverns of Bet Guvrin are a system of underground quarries that were excavated in a soft and discontinuous chalk in central Israel, some 1000 years ago. The caverns form an integral part of a historic site, which serves today as an out of doors archeological museum visited by more than 200,000 tourists per year. The caverns have been exhibiting unstable structural behavior since they were open to the public in the early 1950s, including two cases of global failure in recent

years. Israel Nature and Parks Authority initiated this research in order to study the ongoing failure mechanisms and to consider the long-term stability of the underground structures.

In the Bet Guvrin area more than 800 bell-shaped caverns have been explored by archeologists [1]. Many of the caverns are within the jurisdiction of Bet Guvrin National Park (Fig. 1). The caverns are clustered in a number of complexes, the largest being an assembly of some 200 individual openings. The caverns were excavated during the early Arabic period (7th–11th centuries) as stone quarries. The excavation process usually started from the top, taking advantage of the hard and relatively thick (1–3 m) calcareous caliche layer, locally known as the “Nari” crust. The ancient workers first excavated a vertical shaft of up to 1 m diameter through the hard caliche layer. Upon reaching

\*Corresponding author. Tel.: +972-8-647-2621; fax: +972-8-647-2997.

E-mail address: hatzor@bgumail.bgu.ac.il (Y.H. Hatzor).

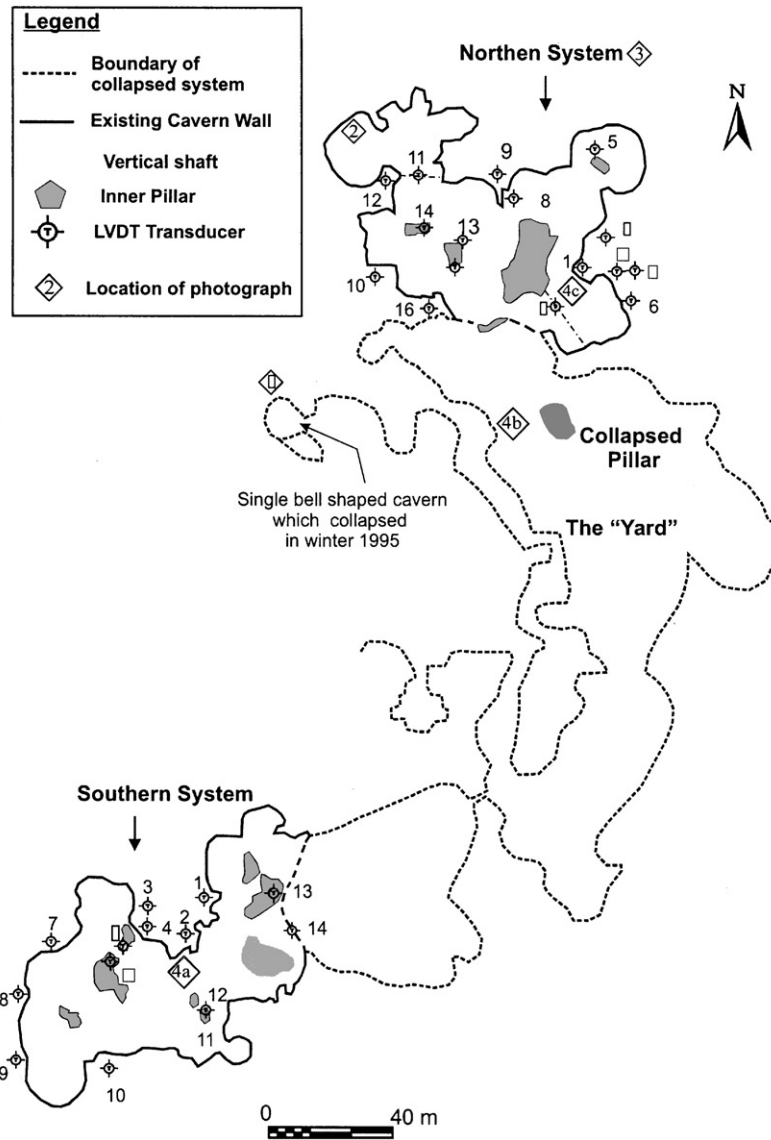


Fig. 1. Layout of the studied complex at Bet Guvrin with location of transducers.

the soft chalk below, the shaft was enlarged as it was deepened, forming a bell-shaped geometry. A single cavern may reach a floor diameter and height of up to 20 m (Fig. 2). Extensive exploitation of a given area led to excessive enlargement of individual caverns in places resulting in overlap of adjacent openings. This process led to the creation of huge underground structures that reach unsupported spans of up to 40 m (Fig. 3).

The caverns were excavated close to the ground surface in close proximity one to another. In some cases the cavern crown is found at a depth as shallow as 4 m. The caverns were excavated through the middle Eocene Maresha formation, which consists of massive, soft, homogeneous, white chalk. The mechanical behavior of Marsha chalk is discussed in great detail by Talesnick et al. [2]. The chalk is horizontally bedded, but distinct



Fig. 2. A complete, un damaged, single Bell-shaped cavern at the Northern system at Bet Guvrin (opening height 12 m).



Fig. 3. Several overlapping caverns—the Southern system at Bet Guvrin (opening height 15 m).

bedding plane surfaces are rarely detected in the field. Nevertheless, mechanical tests clearly show that the chalk exhibits transverse isotropy across sedimentation planes. Consequently, strength and deformation characteristics are highly anisotropic. The chalk is much stronger and stiffer when loaded in parallel to the bedding plane direction (major principal stress axis parallel to planes of isotropy), and much weaker and softer when loaded normal to bedding, both in tension and in compression.

The geometrical characteristics of the caverns yield at least three major sources of instability:

- (1) Close proximity of neighboring caverns results in high tangential stress concentrations in common sidewalls. Under some circumstances these stresses could reach the unconfined compressive strength of the chalk when stressed normal to bedding planes. This problem becomes more acute as opening span increases and as common sidewall thickness decreases. Common sidewalls with thickness as small as 1 m are found in the studied complex.
- (2) The large span of overlapped openings induces tensile stresses tangential to the roof face. Under some circumstances the magnitude of the tensile stresses may reach the tensile strength of the chalk when stresses in directions parallel to bedding planes.
- (3) The relatively small head cover suppresses arching and interlocking mechanisms such that the potential for block instabilities is increased.

Evidence of failure due to all three sources are abundant in the studied complex (Fig. 4).

In this research a cavern complex consisting of 80 individual and overlapping openings occupying an area of 1640 m<sup>2</sup> is analyzed. The studied complex is divided into three distinct areas (Fig. 1):

- The Southern system—a cluster of 16 adjacent and overlapping individual openings.

- The Northern system—a similar cluster of 14 individual openings.
- The Yard—a 70 m wide open pit, bordered by vertical walls, formed amid the caverns, and believed to be the remnant of a system of caverns that collapsed in historical times. Kloner [1] suggests that 50 individual bell-shaped caverns occupied the present Yard area.

### 1.2. Continuous vs. discontinuous stability analyses for underground openings

Weak and discontinuous rock masses are often encountered in underground excavations. In such rock masses local instabilities, which may lead to global failure, are driven primarily by two different and largely independent mechanisms: (1) failure through intact rock elements, (2) displacement of rigid keyblocks from the sidewalls or the roof of the opening. Both failure mechanisms may be active simultaneously resulting in a “mixed failure mode” process. Traditionally, stability analyses are based on a completely continuous or a completely discontinuous approach. The specific method chosen might depend upon the education, personal inclination, experience, and available tools at the hands of the engineer.

When a rock mass is modeled as a continua, numerical solution schemes such as the finite element [3], finite difference [4], or boundary element [5] methods may be applied in order to determine the stress and strain distribution throughout the analyzed domain. These methods may incorporate interface elements [6], however the numerical implementation of such modifications is restricted. Applications of the finite element and the boundary element methods to rock engineering are reviewed by Pariseau [7] and Watson [8]. Cundall [9] discusses the application of the finite difference method.

When a rock mass is modeled as a discontinua, the discrete element method [10] or discontinuous deformation analysis [11] may be applicable. In these methods finite displacements and rotations of discrete elements are allowed, including complete detachment at interfaces. Principles of DEM and DDA are discussed by Hart [12] and Shi [13]. Applications of DDA to underground openings are presented by Yeung [14], Hatzor and Benari [15] and by Kim et al. [16], among others.

Where local instabilities are expected due to movement of unstable blocks, the rigorous analytical solution of Block theory [17] is very useful. Block theory applications to tunneling are discussed by Hatzor and Goodman [18,19] and Tinucci and Funk [20], among others.

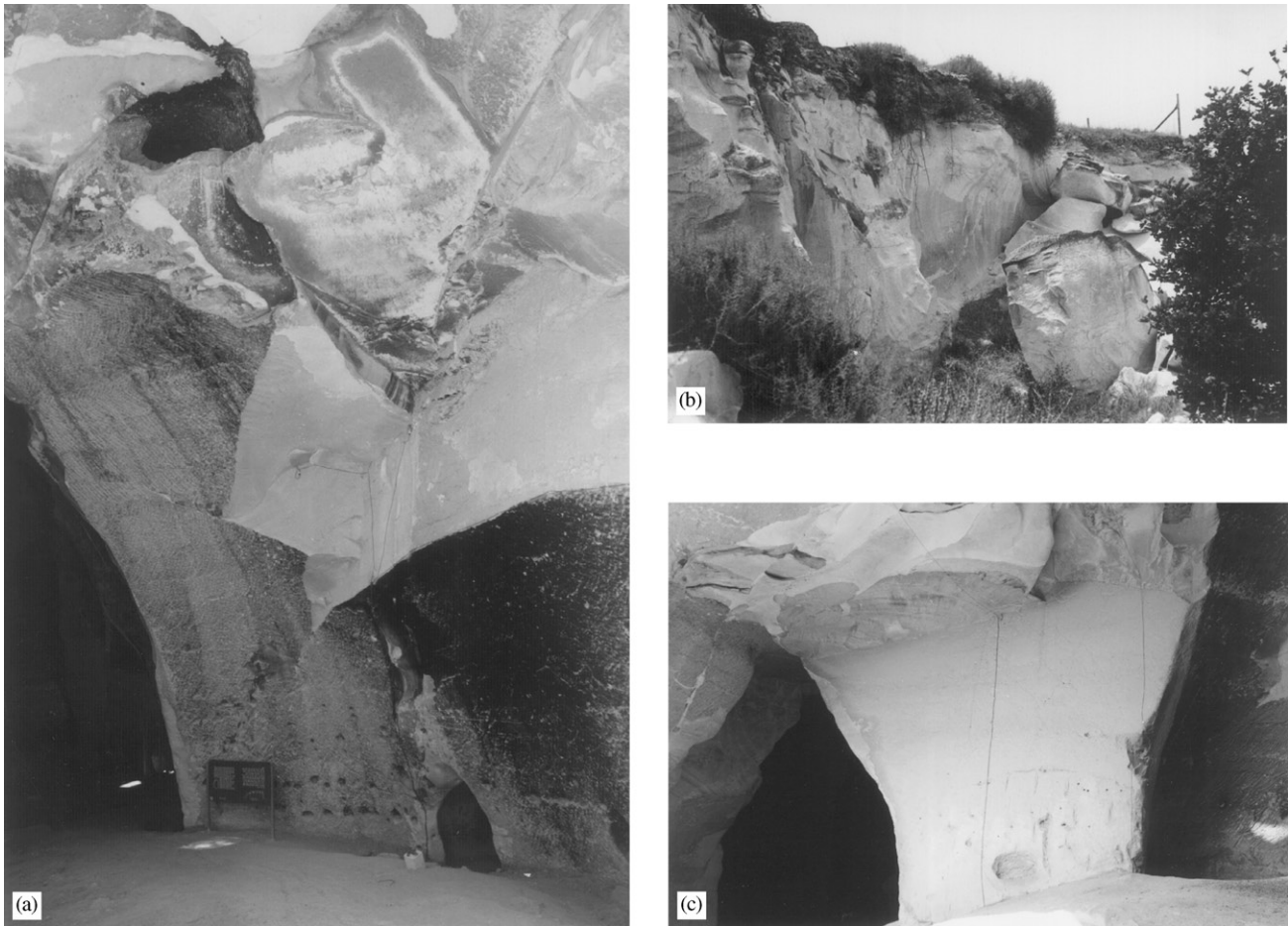


Fig. 4. Failure modes at the studied complex: (a) intact rock fracture at the abutments of the Southern system as indicated by the uneven face surface. The original surface can be identified by characteristic chisel marks and dark patina (opening height 15 m); (b) tensile fracture markings at the boundaries of a system which collapsed in historic times due to excessive tensile stress concentrations (sidewall height 9 m); (c) keyblock failure at the abutment of the Northern system due to relaxation processes (block height 8 m).

In most cases the continuity and discontinuity of the rock mass cannot be decoupled. For example, when a rock mass is largely continuous but contains a few persistent discontinuities, instability may result from exceedingly high stresses in intact rock elements, displacement of removable blocks along pre-existing discontinuities, or a combination of the two (Fig. 4). The latter process is termed here a “mixed failure mode”. The mixed failure mode is particularly dangerous because it may lead to global collapse of the structure. Application of either a fully continuous or a fully discontinuous approach may be inadequate in such cases. The fully continuous methods cannot detect potential instabilities due to movement of individual blocks because they ignore block kinematics. On the other hand, in discontinuous methods (Fig. 5) (DEM, DDA) the resolution of internal stresses inside block elements is less accurate and the possibility of intact rock failure may be overlooked. In block theory internal block stresses are completely ignored.



Fig. 5. A single, small span, bell-shaped cavern which collapsed during the winter of 1995 due to slippage along a pre-existing joint.

In this paper, we show how the application of continuous and discontinuous methods may be integrated using an illustrative case study. We perform a comprehensive stress analysis of different geometrical

cross sections using FLAC. We then perform a comprehensive block theory analysis, identify the critical-key-blocks in the openings, and generate a trace map of expected removable keyblock locations behind the free surface. Finally, we monitor keyblock displacements in potentially unstable zones. Using the stress analysis results, keyblock study, and monitoring data, we establish the governing failure mechanism and locate weak zones, the reinforcement of which should ensure safe and lasting global stability.

### 1.3. Methods of site investigation and stability analysis

The research program utilized existing maps and plans of the studied complex. In some locations detailed surveying was performed specifically for this project in order to obtain reliable dimensions. All detectable (and accessible) joints were measured in the field and attitudes were superposed on maps. Joint length, spacing, and bridge distribution were determined based upon the developed trace maps.

The mechanical response of the intact rock was studied by testing core specimens that were extracted in the field. A portable hand drill was used to extract NX sized ( $2\frac{1}{8}$ " ) core cylinders from the sidewalls of existing openings. These specimens were drilled horizontally, parallel to bedding planes. A heavier drill, mobilized by a small truck, was used to extract 6" diameter cylinders from the floor of a fresh exposure of horizontally bedded chalk. The 6" diameter samples were drilled vertically, normal to the bedding direction. All cores were retrieved from intact rock; the specimens tested represent the response of virgin material unaffected by ongoing failure processes in the openings. From the 6" diameter samples, NX size cylinders both normal and parallel to bedding were extracted. Four different types of mechanical tests were performed:

- uniaxial compression of solid and hollow cylinders,
- radial compression of hollow cylinders,
- torsion tests on hollow cylinders,
- diametric (Brazilian) compression.

The testing program was designed with the aim of considering the response of the intact chalk to stress in directions normal to, and parallel to the orientation of bedding in the field. Tests were performed such that the deformation characteristics, linearity and strength of the material in these two directions could be quantified. Testing to consider the influence of changes in water content on the response of the chalk was also performed.

The distribution of stress around a typical cavern was modeled using FLAC [4]. The computed tangential stresses in the sidewalls and roof were compared with the relevant uniaxial compressive and tensile strength of

the rock. Based on the computed tangential stresses and the anisotropic nature of the rock, zones of potential failure through intact chalk were mapped.

Principal joint set attitudes were determined based on the joint survey performed in the site investigation phase of the research. The measured joint orientations were used as input into block theory analysis, and critical keyblocks [18,19,21] for each opening were defined. Synthetic joint trace maps for the critical keyblock in unrolled tunnel sections were constructed using an algorithm developed by Shi and Goodman [22]. Based on these sections the area of removable keyblocks in the roof was computed.

The actual performance of the studied complex was considered by monitoring keyblock displacement over time, in the two systems. Fourteen and sixteen joint meters (LVDTs) were installed in the Southern and Northern systems, respectively (Fig. 1). Data acquisition was performed over a period of 28 months. Seasonal expansion and contraction of the soft rock mass was evaluated and separated from actual relative displacements of different keyblocks. Keyblock displacements were then used in order to identify potentially unstable zones and failure mechanisms in the caverns.

Superposition of results from the stress distribution analysis, block theory analysis and monitoring data allows for the mapping of potentially troublesome zones within the cavern complex. Mapping of this nature is helpful in considering the mechanics of the ongoing failure processes, and thereby aid in prescribing possible support schemes for ensuring long term stability.

## 2. Rock mass characteristics at Bet Guvrin

### 2.1. Anisotropy, elasticity, and strength of intact specimens of Maresha chalk

The chalk at Bet Guvrin belongs to the Maresha member of the Eocene Avedat Group of central Israel. The chalk is soft, white, and homogeneous, with average porosity of 58% and bulk (dry) density of  $1.1 \text{ g/cm}^3$ . Tsesarsky et al. [23] performed standard uniaxial and triaxial compression tests on solid cylindrical specimens oriented both normal to and parallel to bedding and discussed strength and deformation anisotropy. Talesnick et al. [2] provide additional data on elasticity, strength, and anisotropy of Maresha chalk based on results of radial compression and torsional shear of hollow cylinders, and of Brazilian tests performed on solid discs. The influence of water content on both compressive and tensile strength of Maresha chalk is also explored by Talesnick et al. [2]. Detailed testing methodologies are described in the respective publications.

Uniaxial and triaxial compression tests were performed on NX size samples prepared according to ASTM and ISRM standards regarding end roughness ( $<0.01$  mm), perpendicularity ( $<0.05$  rad), and  $L/D$  ratio ( $\approx 2.0$ ). Testing was performed in a hydraulic, close-loop, servo-controlled, triaxial load frame (Terra-Tek system model FX-S-33090) having a stiffness of  $5 \times 10^9$  N/m. All tests were performed at a constant strain rate of  $10^{-5}$  s $^{-1}$ . Complete stress–strain curves beyond peak stress were obtained in most tests. Axial and radial strains were recorded using two four arm axial and radial strain cantilever sets, with 10% and 7% strain range, respectively, both with 1% linearity full scale.

Typically, bedding or sedimentation planes cannot be detected unaided in hand specimens. Nevertheless, the mechanical response of the chalk is typical of transverse isotropic materials, with the direction of sedimentation corresponding to an axis of material symmetry. Fig. 6 shows a comparison between radial strains computed in mutually perpendicular directions ( $\epsilon_{r1} \perp \epsilon_{r2}$ ) during uniaxial compression testing of six solid cylinders of Maresha chalk. Specimens BG-8A, 9A, and 3D were loaded normal to bedding ( $\beta = 0^\circ$ , where  $\beta$  is the angle between the major principal stress and the normal to

bedding). Specimens BG 14.1, 14.2, and 30D were loaded parallel to bedding planes ( $\beta = 90^\circ$ ). Radial deformations of specimens loaded perpendicular to bedding ( $\beta = 0^\circ$ ) were measured in two mutually perpendicular directions both aligned within the plane of bedding. Radial deformations of specimens loaded parallel to bedding ( $\beta = 90^\circ$ ) were measured in two mutually perpendicular directions, one across the bedding planes (along the axis of material symmetry) and the second parallel to the chalk bedding. Table 1 lists the coefficients determined from linear regression of each pair of radial strains as determined for each test. The data suggest that the radial strains inferred in specimens loaded normal to bedding are identical and independent of orientation with respect the axis of the specimen. Conversely, the radial strains inferred from testing of specimens loaded parallel to bedding planes are clearly dependent upon angular orientation with respect to the axis of material symmetry, which seems to be aligned with a direction normal to bedding. These observations serve as experimental confirmation that the direction of sedimentation is in fact the axis of rotational isotropy. Material response within planes parallel to bedding will be different from that displayed in planes oblique or normal to bedding.

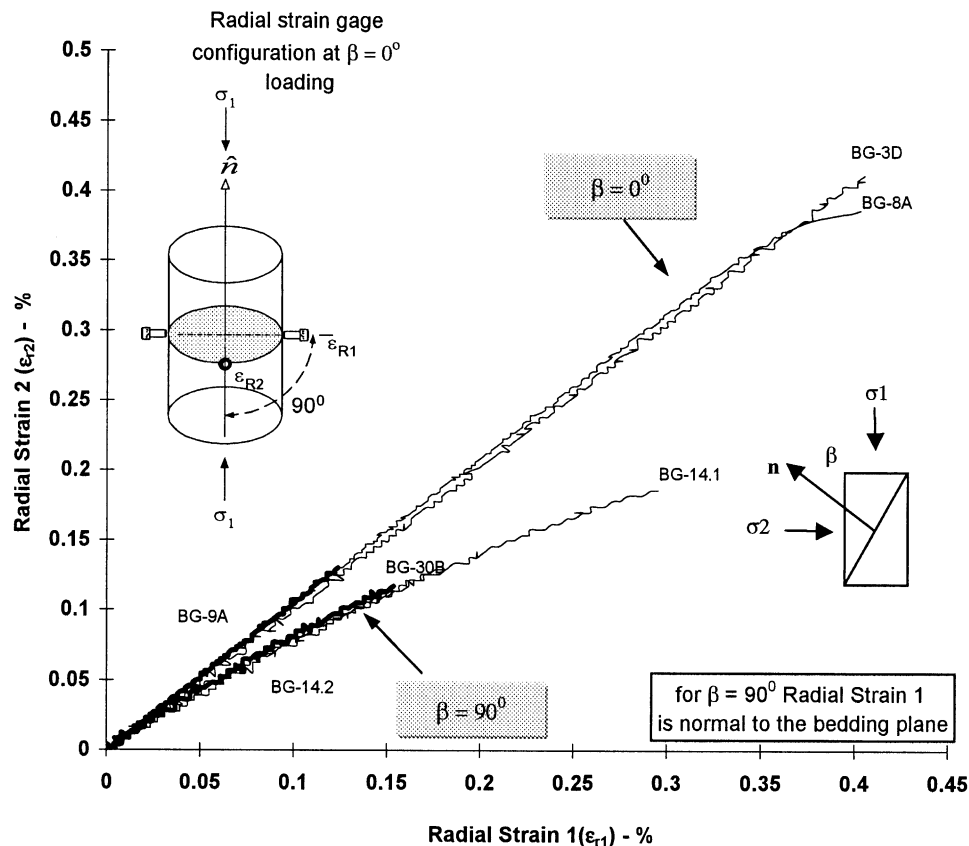


Fig. 6. Experimental confirmation of transverse isotropy along bedding planes for Maresha chalk. Output of two orthogonal radial strain transducers during uniaxial compression under normal ( $\beta = 0^\circ$ ) and parallel ( $\beta = 90^\circ$ ) loading.

The material exhibits strong elastic and strength anisotropy. Fig. 7 shows two complete stress–strain curves of representative solid cylinders of Maresha chalk, one loaded in parallel to bedding ( $\beta = 90^\circ$ ) and the second loaded normal to bedding ( $\beta = 0^\circ$ ). The material is clearly much stronger when loaded parallel to bedding, with peak strength of 9 MPa, compared to 6 MPa when stressed normal to bedding. Since bedding in the field is horizontal, parallel loading ( $\beta = 90^\circ$ ) conditions prevail in the roof of the caverns while normal compression ( $\beta = 0^\circ$ ) prevails in the abutments.

The instantaneous modulus of deformation of the chalk exhibits non-linearity as well as anisotropy. A continuous reduction in the modulus and a continuous increase in Poisson’s ratio accompany the increase in axial stress during uniaxial compression (Fig. 8). The

chalk stiffness when loaded in parallel to bedding is approximately 60% higher than the chalk stiffness when loaded normal to bedding (Fig. 7).

The effect of water content on strength and deformability was studied by Talesnick et al. [2]. The results (Fig. 9) illustrate the reduction in compressive strength with increasing water content. The degree of strength anisotropy was found to remain constant (dashed line in Fig. 9) over a range of water contents ( $\omega = 3\text{--}50\%$ ). The effect of water content on the modulus of deformation was shown to be severe, small increase in water content result in drastic reduction in material stiffness.

The tensile strength of Maresha chalk was studied by testing solid disks in diametrical (Brazilian) compression [2]. The influence of water content on tensile strength was investigated as well. Fig. 10 summarizes results of Brazilian tests where the tensile component of stress developed in directions parallel to bedding. The peak tensile strength was found to be approximately 1 MPa at a water content of 3%. Small changes in water content from  $\omega = 3\%$  to 10% drastically reduce the tensile strength of the chalk. The loss of strength over the water content range of  $\omega = 10\text{--}40\%$  is much less severe.

In the stability analysis we have used a mean uniaxial compressive strength of 9 and 6 MPa for parallel and normal compression, respectively, and a tensile strength of 1 MPa in directions parallel to bedding.

Table 1  
Relationship between two orthogonal radial strain outputs during uniaxial compression of solid cylinders in Maresha chalk

Sample	$\beta$ , geometry	$R^2$	Slope
BG-3D	$0^\circ$	0.999	1.07
BG-8A	$0^\circ$	0.999	1.04
BG-9A	$0^\circ$	0.999	1.11
BG-14.1	$90^\circ$	0.980	0.7
BG-14.2	$90^\circ$	0.991	0.81
BG-30D	$90^\circ$	0.996	0.75

$\beta = 0^\circ$ —compression normal to bedding,  $\beta = 90^\circ$ —compression parallel to bedding.

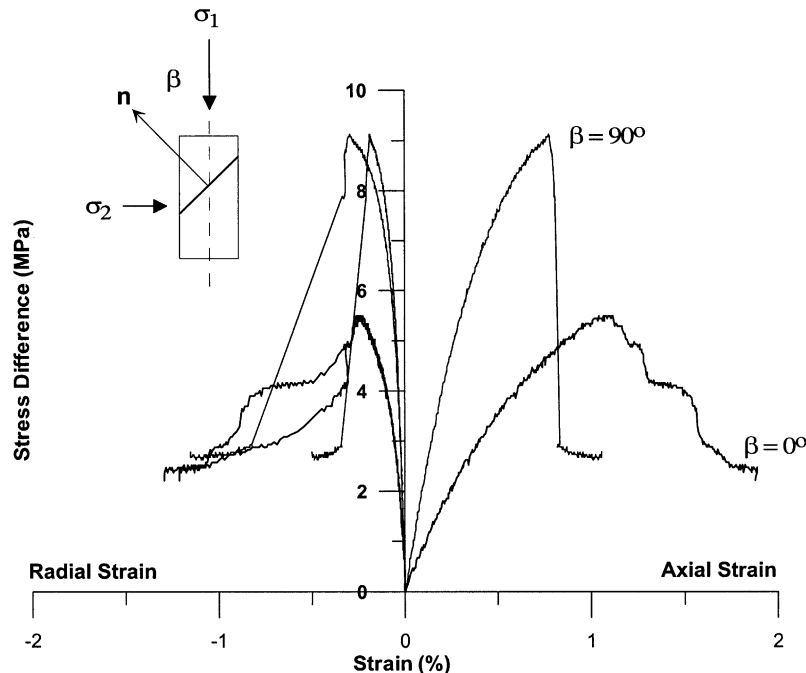


Fig. 7. Ultimate strength and elastic anisotropy for Maresha chalk—results of two representative uniaxial compression tests.

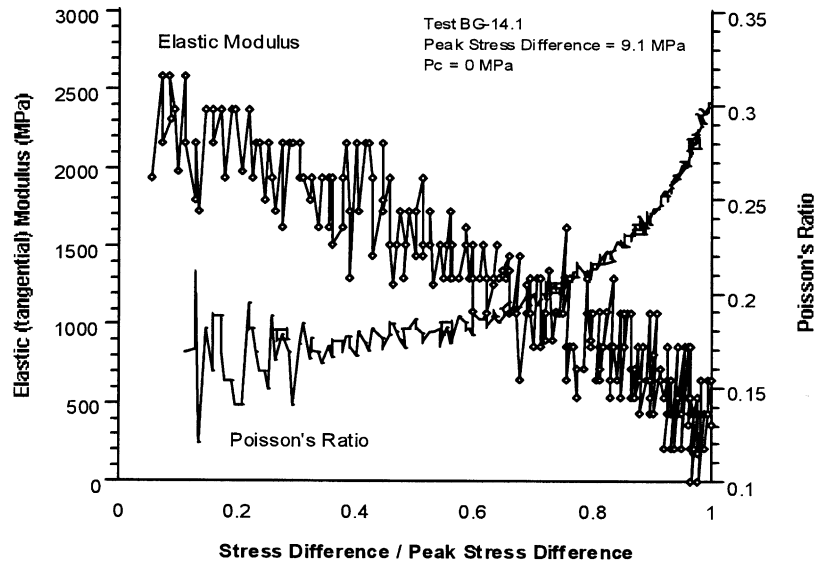


Fig. 8. Elastic non-linearity of Maresha chalk.

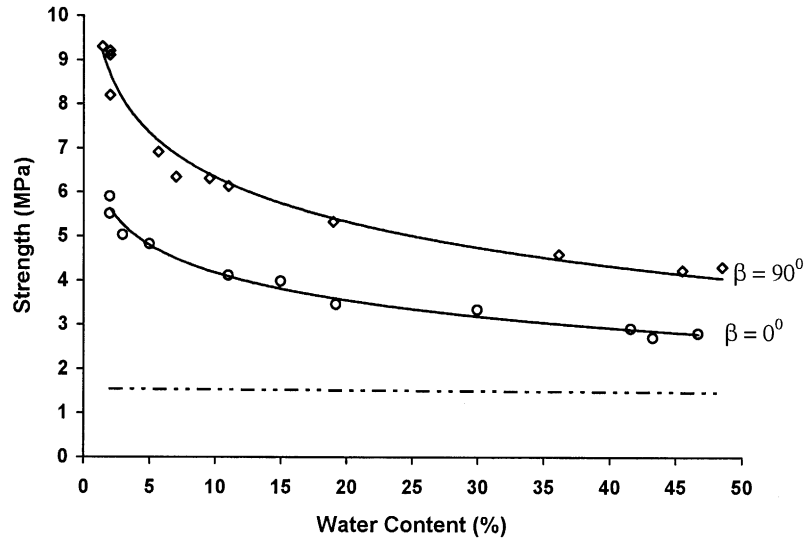


Fig. 9. Influence of water content on uniaxial compressive strength of Maresha chalk (after Talesnick et al. [2]). The strength ratio ( $\sigma_{c\beta=90} / \sigma_{c\beta=0}$ ) is shown in dashed line.

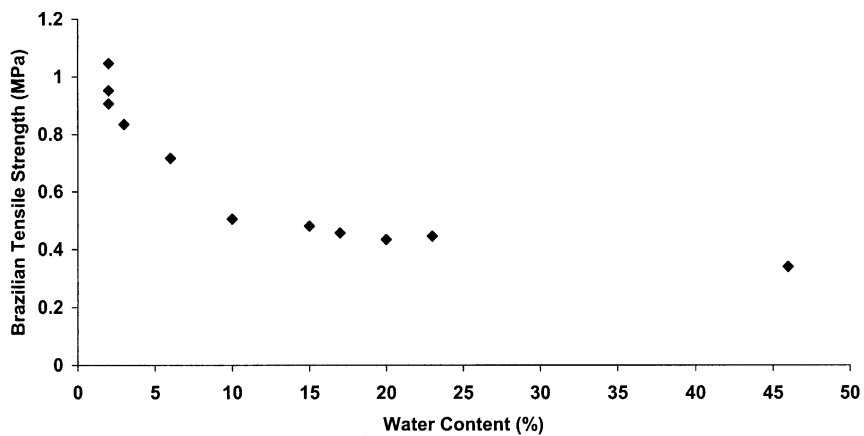


Fig. 10. Influence of water content on Brazilian tensile strength of Maresha chalk in direction parallel to bedding (after Talesnick et al. [2]).

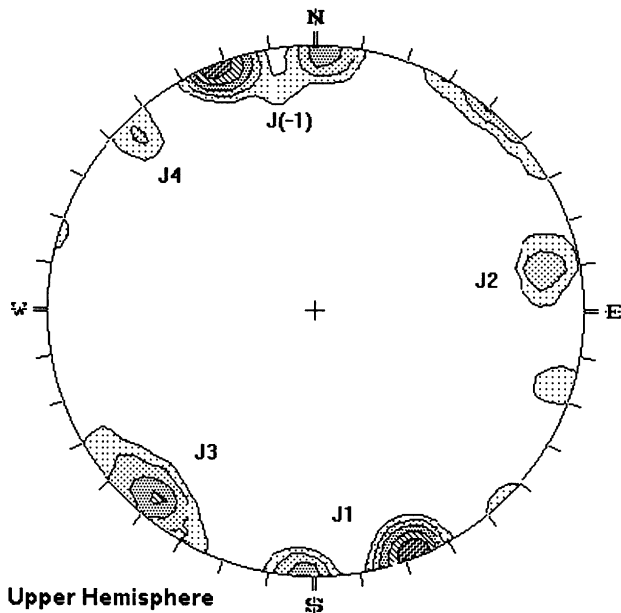


Fig. 11. Upper Hemisphere stereographic projection of poles measured at the studied complex at Bet Guvrin (106 entries).

Table 2  
Principal joint sets, frequency and mean spacing at the Bet Guvrin bell shaped caverns

Joint set no.	Mean attitude (dip/dip direction)	Frequency (1/m)	Mean spacing (m)
1	85/170	0.19	5.26
2	80/80	0.11	9.1
3	80/220	0.23	4.25
4	85/315	0.1	10

## 2.2. Rock mass structure

The discontinuities at Bet Guvrin are primarily clean joints with little or no in filling material. The joints are very persistent and widely spaced. Bedding planes are rare or entirely absent on the rock mass scale and are not regarded as a discontinuity in the analysis. The contact between the overlying caliche (Nari) layer and the chalk is wavy and open in places. It has been regarded as a single horizontal discontinuity surface, which transects the rock mass 2 m below ground surface.

A total of 103 discontinuities were mapped in the studied complex, 55 joints in the Northern system and 48 in the Southern system. Many joints transect the caverns and exhibit trace lengths of tens of meters, the persistence of which is therefore assumed to exceed the boundaries of the problem domain. Four principal joint sets were identified (Fig. 11), the principal direction and (corrected) frequency of which are shown in Table 2.

## 2.3. Predictive capabilities of $Q$ and $RMR$

Traditionally, rock engineers have assessed the stability of underground openings, stand up time, and required support pressures on the basis of empirical rock mass classification methods, of which the  $Q$  [24] and  $RMR$  [25] are the most widely accepted. This has been attempted in the current study, using the site investigation and mechanical test data described above. Since the mechanical behavior of the rock exhibits anisotropy, two scenarios were considered as input parameters:

- Case 1—stronger rock mass (parallel loading  $-\beta = 90^\circ$ , active in roof),
- Case 2—weaker rock mass (normal loading,  $\beta = 0^\circ$ , active in abutments).

The results for  $RMR$  and  $Q$  classifications are listed in Tables 3 and 4, respectively.

The  $RMR$  values are in the range of 46–70 depending on loading condition. According to these values a single bell-shaped cavern of up to 10 m span would be expected to sustain a stand up time of days in the weaker case ( $\beta = 0^\circ$ ), and up to 1 year in the stronger case ( $\beta = 90^\circ$ ). A system of overlapping caverns with a total active span of 20 m or more would have been expected to undergo immediate collapse according to the  $RMR$  assessment.

The sensitivity of the  $Q$  system to strength can be studied through the  $SRF$  parameter which incorporates the strength/stress ratio ( $\sigma_c/\sigma_1$ ), provided that a stress analysis is performed. If we consider a typical cavern with an active span of 24 m and height of 8 m the strength/stress ratio at the sidewall and roof is 17 and 36, respectively, assuming that the maximum tangential stresses at the sidewall and roof are 350 and 250 kPa, respectively (see Section 3 below). Both strength/stress ratios are within the range of 200–10 and therefore return the same  $SRF$  Value of 1.0. It is not possible to consider the loading condition in all other  $Q$  parameters and therefore the  $Q$  values for a complete cavern (both roof and abutments) remained the same. Our estimations return a  $Q$  value of 12 for the caverns at Bet Guvrin (Table 4).

If we consider an excavation support ratio ( $ESR$ ) of 0.8, suitable for public facilities, the maximum unsupported span would be about 5 m. If we consider an  $ESR$  of 5, suitable for temporary mine openings, the maximum unsupported span would be about 30 m. Surprisingly, the predicted unsupported span by  $Q$  is not far from the unsupported spans that are found in the park assuming an  $ESR$  suitable for temporary mines. Considering the original purpose of the caverns an  $ESR$  of 5 would have been appropriate because the caverns were designed as temporary underground quarries and not as long-term public or dwelling facilities.

Table 3  
RMR classification for Maresha chalk considering mechanical anisotropy with respect top strength

	$\beta = 90^\circ$ (Cavern roof)	Rating	$\beta = 0^\circ$ (Cavern abutments)	Rating
Uniaxial compressive strength	9 MPa	2	6 MPa	1
RQD	> 90%	20	> 90%	20
Spacing	> 2 m	20	> 2 m	20
Condition of discontinuities	Slightly rough surface, separation < 1 mm, slightly weathered wall	16	Slightly rough surface, separation < 1 mm, slightly weathered wall	16
Groundwater condition	Dry	12	Wet	7
Orientation of discontinuities	Very favorable	0	Very Unfavorable	-12
<i>RMR</i>		70		46

Table 4  
*Q* classification for Maresha chalk considering mechanical anisotropy with respect top strength—a single bell shaped of typical height and diameter is considered ( $H = 12$  m,  $D = 16$  m)

	$\beta = 90^\circ$ (Cavern roof)	Rating	$\beta = 0^\circ$ (Cavern abutments)	Rating
RQD	Excellent	90	Excellent	90
Number of joint sets ( $J_n$ )	4	15	4	15
Roughness ( $J_r$ )	Smooth undulating	2	Smooth undulating	2
Degree of alteration ( $J_a$ )	Unaltered	1	Unaltered	1
Water inflow ( $J_w$ )	Dry excavation	1	Dry excavation	1
Stress reduction factor ( $\sigma_c/\sigma_1$ )	$9000/250 = 36$	1	$6000/350 = 17$	1
<i>Q</i>		12		12

The complex of bell-shaped caverns at Bet Guvrin presents an ideal opportunity to consider the applicability of empirical classification methods as design tools in soft and discontinuous rock. The distinction made here between a stronger and weaker case is of course artificial, since in reality both loading conditions are operating in a single opening simultaneously due to the inherent anisotropy of the compressive strength. The separation into two scenarios has been made in order to accommodate the limitation of empirical classification methods which assign a singular strength value to the entire rock mass.

Data collected from the site suggest that the *RMR* system is overly conservative in this case while the *Q* system provides more realistic predictions. Many singular caverns and systems of overlapping caverns with free spans greater than 10 m are free of signs indicative of distress. This even though they have been unsupported for more than 1000 years. Nevertheless, many bell-shaped caverns have collapsed over the 1300 years history of Bet Guvrin and some cavern systems are experiencing on going failure processes. Therefore, the conservative result of *RMR* is not entirely unwarranted. Finally, it should be remembered that both *RMR* and *Q* were not meant to replace actual engineering analysis but rather to provide better understanding of the rock mass. This case study shows that descriptive rock mass

classification effort provides relatively good insight to the nature and quality of the rock mass at hand, however it could not, and should not, stand alone as a design tool.

### 3. Stress distribution assuming the chalk to be a continuous rock mass

The stress distribution around the caverns has been calculated assuming the chalk to be a continuous rock mass using FLAC 3.3 [26], a 2-D explicit, finite difference scheme. Two loading configurations have been modeled:

- axis-symmetric configuration—for single bell-shaped opening,
- plane strain configuration—for elongated system of overlapping caverns.

The constitutive model, material constants, far field stresses and boundary conditions were identical for the two loading configurations. The chalk was modeled as a transversely isotropic solid where the axis of material symmetry is aligned with the vertical. The unit weight of the chalk was set at  $12 \text{ kN/m}^3$ , and the modeled elastic constants were based upon secant moduli at 50% of the

dry uniaxial compressive strength. The far field stresses were set based upon gravitational loads under at-rest lateral stress conditions. A uniform vertical stress of 40 kPa was applied at the ground surface simulating a 2 m thick layer of the caliche (Nari) crust. A schematic representation of the modeled geometry and assigned boundary conditions is shown in Fig. 12.

### 3.1. Single bell-shaped cavern

Typically, singular caverns at the park exhibit major and minor semi-axes of 16 and 12 m corresponding to a free span and height of 16 and 12 m, respectively. From the axis symmetric computation the maximum vertical stress develops at the base of the abutments, with a magnitude of  $\sigma_{yy} = -350$  kPa (Fig. 13a). This stress acts normal to bedding and must be compared with the mean peak compressive strength at  $\beta = 0^\circ$  loading, which is 6 MPa for dry conditions. The factor of safety (FS) against failure in compression at the lower abutments of single caverns is therefore estimated at 17. The maximum horizontal stress develops at the roof with a

magnitude of  $\sigma_{xx} = -250$  kPa. This value must be compared to the mean uniaxial compressive strength at  $\beta = 90^\circ$  loading, which is 9 MPa in dry conditions. The FS against failure in axial compression in the roof of a single opening is 36 (see Table 5).

The conclusion from the axis symmetric analysis is that isolated, single bell-shaped caverns at Bet Guvrin, are safe against structural failure due to stress concentrations.

### 3.2. System of overlapping caverns

A system of adjacent and overlapping single caverns cannot be modeled precisely, either in 2D or in 3D, due to its intricate geometry. Based on field mapping of the larger southern system in the studied complex, we have chosen to model the encompassing envelope of the system as a single tunnel having elliptical cross section with major and minor semi axes of 15 and 17 m respectively. These values translate to a span of 34 and

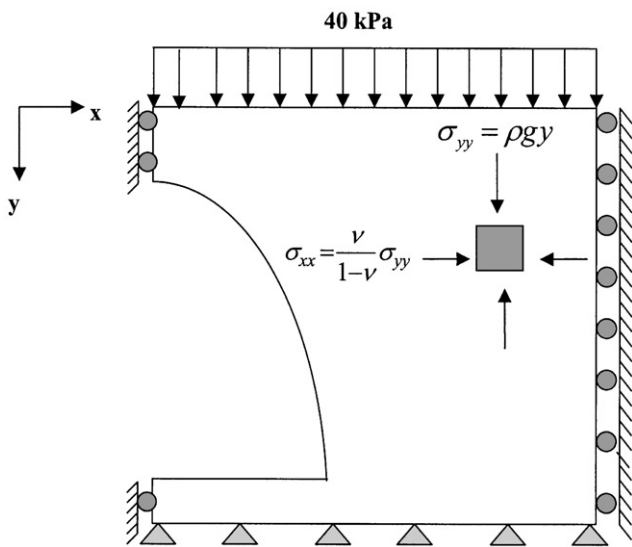


Fig. 12. Initial and boundary conditions used in numerical modeling.

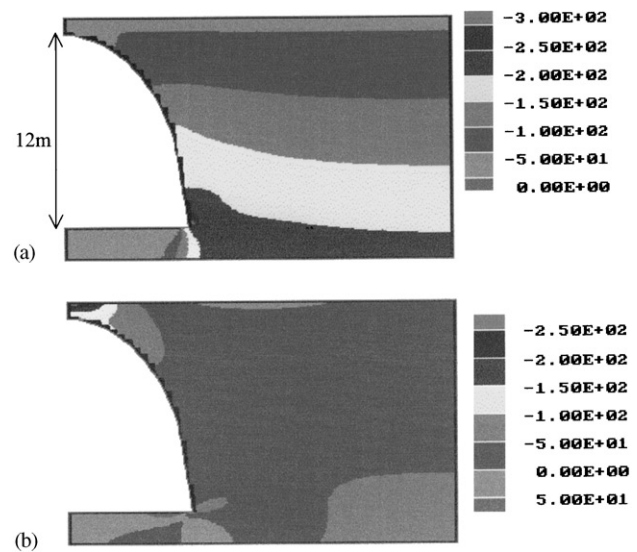


Fig. 13. Stress distribution (axis-symmetric configuration) around a single bell-shaped cavern, elliptical cross-section with 16m diameter and 12 m height: (a) vertical stresses ( $\sigma_{yy}$ ), (b) horizontal stresses ( $\sigma_{xx}$ ). Stress units in kPa, compression negative.

Table 5  
Concentrated results of stress analysis using FLAC

Cavern geometry	Loading configuration	Failure mode and factor of safety dry conditions			
		Crushing at abutments	Crushing at roof	Crushing at common side wall	Tensile fracture at upper roof
Single cavern	Axis symmetric	17	36		
Overlapping caverns	Plane strain	6	12		4
Two adjacent caverns	Plane strain			3	
Single cavern after collapse of common side wall	Plane strain	4	2		0.5

15 m height. The plane strain computation results in maximum vertical stresses which develop at the abutment with a value of  $\sigma_{yy} = -1$  MPa, and the maximum horizontal stress develops at the crown with a value of  $\sigma_{xx} = -750$  kPa. Finally, horizontal, tensile, stress concentrations develop at two locations in the large opening: above the curved segment of the roof and immediately at the face of the roof, with a maximum magnitude of  $+250$  kPa (Fig. 14). These tensile stresses must be compared to the tensile strength parallel to bedding which is about 1 MPa in dry conditions. The development of tensile stresses is alarming because of the relatively low tensile strength of the rock and its sensitivity to changes in water content. The respective factors of safety against failure in axial compression at the abutment and against failure in compression or tension in roof are listed in Table 5.

The stability of an overlapping system is lower than that of a single cavern by a factor of about 3, and in addition tensile stresses develop at the roof. Nevertheless, the stress analysis clearly indicates that such spans are essentially safe. Even when we consider strength degradation due to increased water content, the strength loss would be up to a factor of 2.0 and the respective factors of safety would still indicate long-term stability.

This result is only partially supported by field evidence. Both the Southern and Northern systems fall into the category of high span overlapping structures. Both systems have been standing unsupported for at least 1000 years. In that respect we can claim that the numerical result is rather reliable. However, in both systems there is ample evidence for ongoing failure processes, which have not developed to full-scale global

failure, but certainly endanger the long-term stability of the systems. The failure processes are detected by irregular fracture markings on the sidewalls, and by monitored keyblock displacements.

### 3.3. Two adjacent openings

At many locations in the park two adjacent bell-shaped caverns share a common sidewall. The sidewall thickness may vary from several meters to less than a meter. It is interesting to investigate the level of stress concentration in a common wall as a function of wall thickness, and to see at which sidewall thickness the vertical stress concentration becomes excessive.

Two adjacent openings with individual geometric characteristics as found in several locations at the park are shown in Fig. 15. The calculated vertical stress in the common sidewall is  $\sigma_{yy} = -2$  MPa for sidewall thickness of 3 m. In this configuration the FS against crushing failure at the abutment (dry conditions) drops to 3 (Table 5).

When the common sidewall thickness drops to 2 m the vertical (compressive) stress increases to  $\sigma_{yy} = -3$  MPa and consequently the FS against crushing failure in the abutment drops to 2. With this level of FS, the modeled system could collapse upon substantial wetting of the rock mass during wet periods. Indeed, common sidewalls thinner than 3 m are rare in the studied complex. When the common sidewall thickness approaches 3 m local damage can be detected in situ, and the original chisel marks which were left neatly on the freshly excavated face by the ancient workers are absent. Instead, irregular corners and uneven surfaces are abundant (Fig. 4a).

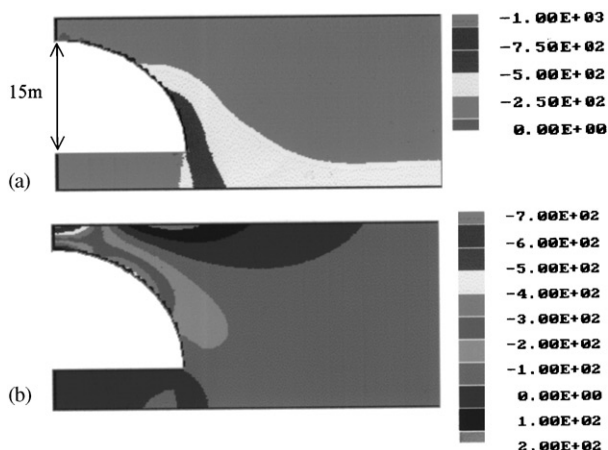


Fig. 14. Stress distribution around a system of overlapping bell-shaped caverns, modeled as a tunnel of elliptical cross-section (plane strain configuration), with 34 m diameter and 15 m height: (a) vertical stresses ( $\sigma_{yy}$ ), (b) horizontal stresses ( $\sigma_{xx}$ ). Stress units in kPa, compression negative.

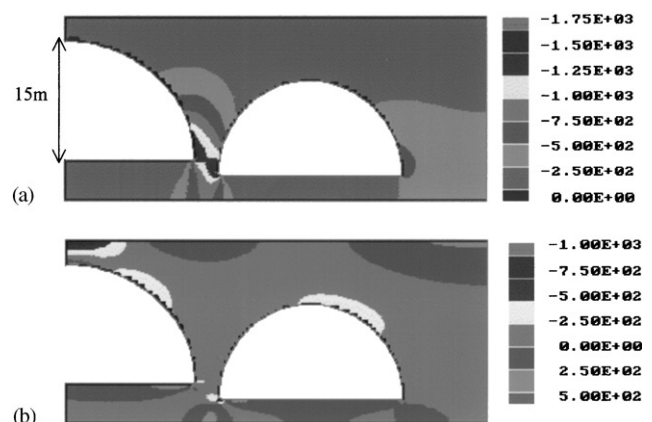


Fig. 15. Stress distribution around two adjacent parallel systems of bell-shaped caverns, each system modeled as a tunnel (plane strain configuration), with a 3 m thick common wall: (a) vertical stresses ( $\sigma_{yy}$ ), (b) horizontal stresses ( $\sigma_{xx}$ ). Stress units in kPa, compression negative.

### 3.4. Stability of adjacent caverns after common sidewall failure

When the common sidewall between two original caverns is too thin it may fracture and disintegrate as a result of excessively high compressive stresses. In such an event, a single freestanding opening with a very large span may form. Such cases of combined openings are common at Bet Guvrin. The combined structure modeled here has a free span of 61 m. The plane strain computation results in compressive stresses of  $-1.5 \text{ MPa}$  at the abutments, below the available strength of  $6 \text{ MPa}$ . Similarly, compressive stresses of  $5 \text{ MPa}$  develop at the roof. Since the dry strength in parallel loading is  $9 \text{ MPa}$  the roof of the combined structure is safe from crushing failure as well.

While the sidewalls and immediate roof of the combined structure are safe against failure in compression (while dry), high horizontal tensile stresses develop above the smaller opening, near the interface with the Nari cover, with a magnitude of  $\sigma_{xx} > +2 \text{ MPa}$ , twice the tensile strength in parallel loading ( $\beta = 90^\circ$ ). This result implies that failure of common sidewall by axial crushing will be followed by development of exceedingly high tensile stresses at the roof of the combined structure. Consequently, tensile fracture propagation may possibly lead to global failure. The factors of safety for the different failure modes are listed in Table 5.

To summarize, in the case of common sidewall failure (Fig. 16), a freestanding opening with unsupported span of  $61 \text{ m}$  may develop momentarily. Such a large unsupported span will lead to the development of excessive tensile stresses in the upper roof, which may induce tensile fracture propagation from the upper roof and down to the free surface. Once the propagated

fracture meets the immediate roof, global failure will be inevitable. This is the progressive failure scenario assumed to have been active in the failure of the “Yard” at Bet Guvrin (Fig. 1). Traces of tensile fractures in the upper roof of the original cavern are shown in Fig. 4b.

## 4. Block theory analysis in discontinuous rock

The stress analysis based upon the assumption of a continuous rock mass may account for some of the failure processes, which have been active at Bet Guvrin. Nevertheless, several cavern failures cannot be accounted for by the stress analysis discussed above. The computed stresses are in many cases insufficient to initiate failure of the intact rock, either in tension or in compression. For example, Fig. 5 presents a single bell-shaped cavern that failed in the mid-1990s. The stress concentrations computed for the original cavern geometry were well below the critical values, for either wet or dry conditions. Displacement along discontinuities in the rock mass controlled the failure shown in Fig. 5. In this section the significance of keyblock failures is explored by means of the “critical keyblock analysis”.

### 4.1. Critical keyblock analysis

The critical keyblock analysis and its application to tunneling is discussed by Hatzor and Goodman [18,19]. Some modifications have been presented by Hatzor [21]. The critical keyblock in a given rock mass structure is defined per specific free surface as: “the block which is most likely to develop statistically, and which is least stable mechanically, in the entire outcome space of theoretically removable blocks”. The analytical procedure must be repeated for different free surfaces in a studied underground structure. The results of the critical key block analysis for the roof of the Southern system are shown in Table 6.

The roof of the Southern system (Fig. 1) shall serve as the analyzed free surface in this example. The first step in the analysis is the determination of the principal joint sets in the rock structure. The mean attitude and spacing in each joint set for the rock mass structure at Bet Guvrin were discussed above and are listed in Table 2. Next, all removable JPs [17] for the analyzed free surface must be determined using standard block theory procedures. Note that the rock structure at Bet Guvrin consists of four different joint sets (Fig. 11). Therefore there could be four different joint combinations of three different joints, or a single joint combination of four different joints [19]. In general, the number of possible joint combinations ( $N_{jc}$ ) is given by  $N_{jc} = [n! / (k!(n - k)!)]$  where  $n$  is the total number of joint sets in the rock mass and  $k$  is the number of joints in a joint combination. Tetrahedral blocks, which are comprised

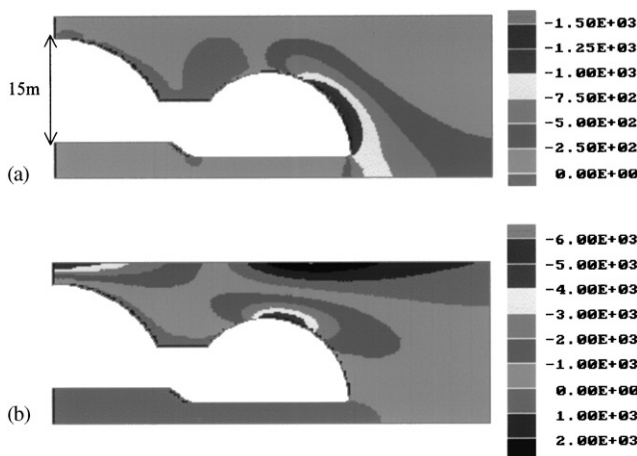


Fig. 16. Stress distribution around a single system formed by the failure of the common wall in Fig. 15 (plane strain configuration): (a) vertical stresses ( $\sigma_{yy}$ ), (b) horizontal stresses ( $\sigma_{xx}$ ). Stress units in kPa, compression negative.

Table 6  
Critical keyblock analysis for the roof of the Southern system at Bet Guvrin

$JC$	$J_i; J_j; J_k$	Removable JP	Mode	$P(JC)$	$F$	$P(B)$
1	123	011	1	0.0012	0.945	0.001134
2	124	111	0 (Falling)	0.0005	1	0.005
3	134	101	12	0.0002	0.845	0.000169
4	234	111	0 (Falling)	0.0009	1	0.0009

$P(JC)$  = joint combination probability,  $F$  = JP instability parameter,  $P(B)$  = block failure likelihood. The critical keyblock in the roof is formed by JP 011 in joint combination 1.

of three joints and one free surface, have been observed to be the most frequent combination in underground openings [27]. This is so because the joint combination probability ( $P(JC)$ ) rapidly decreases with increasing number of joint sets [27]. This expectation was validated empirically in two tunnel case histories [18,19] and a dam abutment case [28]. Therefore, tetrahedral blocks with three bounding joints and a single free surface are typically analyzed in the critical keyblock methodology.

Four different joint combinations are listed in Table 6. The removable JP from the roof for each joint combination is listed in the third column where 0 and 1 indicate upper and lower half-spaces, respectively. The mode of failure from the roof for each removable JP is listed in the fourth column where mode  $i$  indicates sliding on plane  $i$ , mode  $ij$  indicates sliding on planes  $i$  and  $j$  simultaneously, and mode 0 indicates falling or lifting from all joints. The block failure likelihood  $P(B)$ , computed for each removable JP in the roof, is a product of two independent parameters: the joint combination probability  $P(JC)$  and the instability parameter  $F$ . The critical keyblock is the removable block, which has the highest block failure likelihood. The mathematical expressions for  $P(JC)$  and  $F$  are found in Hatzor [21].

A further complication exists in the particular system examined at Bet Guvrin. The base of the Nari crust is of infinite extent with respect to the span of the openings. It transects the rock mass horizontally, in some instances it comes in close proximity to the crown of the openings. The critical keyblock in the roof is therefore a truncated tetrahedral, formed by the combination of the upper half-space of joint set 1, the lower half-spaces of joint sets 2 and 3, the upper half space of the roof surface, and the lower half space of the Nari layer (Fig. 17).

The shape of the critical key block in the roof of the Southern system is shown in Fig. 17 where the maximum keyblock is plotted. For such a case the lines of intersection between the bounding joints are tangent to the opening surface. The maximum key block encompasses maximum volume and roof surface area. The same block geometry can occupy smaller volumes and roof surface areas, depending upon the spacing between the joints.

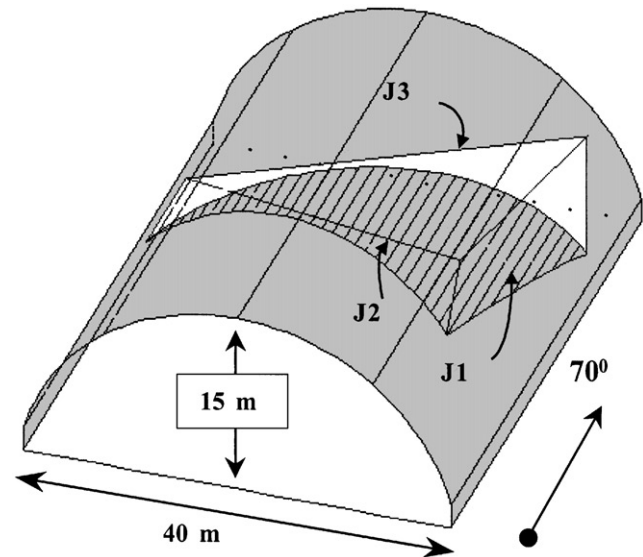


Fig. 17. The critical key block in the roof of the Southern system at Bet Guvrin: maximum keyblock size.

#### 4.2. Removable keyblock area in the roof

The treatment presented thus far has been entirely deterministic, for a single event of the critical keyblock as shown in Fig. 17. In reality however, the roof will be covered by repetitions of the critical keyblock but of different sizes, depending upon the spacing between the joints, and the theoretical block size distribution. Analytical expressions for block size distributions for 2D and 3D cases were previously discussed [29,30] with some simplifying assumptions regarding tunnel shape, joint persistence, and joint orientation. These theoretical studies have shown that the maximum keyblock size has the lowest probability for a given joint set spacing, joint attitude, and tunnel shape.

In this study, a statistical joint trace simulation algorithm [22] was used to generate the discontinuous mesh in the roof. Eight different simulations were performed for the statistical occurrence of the critical keyblock in the roof of the Southern system. In each simulation the traces of the three joint sets were generated using mean length, mean spacing, and mean bridge size. The same proportions between the spacing

Table 7  
Eight different simulations for the removable keyblock area in the roof of the Southern system

Simulation #	$S_1$ (m)	$S_2$ (m)	$S_3$ (m)	Removable keyblock area in the roof (% of total roof area)
1 (maximum key block)	40	14.5	14.5	0.13
2	35	12.74	12.74	0.36
3	30	10.92	10.92	
4	25	9.1	9.1	0.88
5	20	7.28	7.28	4.37
6	15	5.46	5.46	11.77
7	10	3.64	3.64	24.91
8	5	2	2	44.35

$S_i$  is the true spacing of joint set  $i$  in meters. Simulation is performed for an elongated tunnel using the unrolling code of Shi and Goodman [22]. The case of the Southern system at Bet Guvrin is represented by simulation 8.

of the three sets were maintained for each simulation (Table 7). Once generated the trace maps were plotted on unrolled tunnel segments. The half-space combinations belonging to the critical keyblock were identified and tagged. All other half-space combinations were removed. This procedure results in a plot defining the roof area covered by removable joint pyramids for each simulation. A result for a single simulation (simulation 7 in Table 7) is shown in Fig. 18.

The total removable keyblock area obtained in each simulation, divided by the total area of the analyzed roof, varies with mean joint spacing. Smaller joint spacing values lead to a larger removable keyblock area in the roof and larger joint spacing values lead to relatively smaller removable keyblock area in the roof (see Table 7 and Fig. 19). This result is in agreement with the analytical results for keyblock size distribution [29,30], which predict increasing probability for decreasing block size.

We have shown that statistical simulations of joint trace maps together with keyblock theory enable estimation of removable keyblock area in the roof as a function of mean joint spacing. For example, the mean spacing of  $J1$  in the Southern system is 5.26 m. With proportional spacing for the other two joint sets the unrolling procedure indicates that as much as 45% of the roof area is expected to be made up of removable keyblocks (Shaded row in Table 7).

As long as arching stresses are transmitted through the roof the removable keyblocks can remain stable due to mobilization of shear resistance along block boundaries. However, time dependent failure processes either by tensile fracture or local crushing may degrade the compressive arch at the roof and keyblock displacements may ensue. If the block displacement process develops to block failure then global collapse

may follow. Therefore, minute keyblock displacements in the roof may be precursors of a greater progressive failure process, while static keyblocks in the roof may suggest effective arching and long-term stability. In the next section we describe monitoring program that was executed by us in the studied complex over a 2-year period, in order to detect keyblock displacements.

## 5. In-situ monitoring of keyblock displacement

In an attempt to better understand the in-situ response and the ongoing failure processes a comprehensive block monitoring system was installed. Thirty joint meters were installed in the two systems: 16 in the northern system and 14 in the southern (Fig. 1). The joint meters were LVDT-type transducers with a full scale of 20 mm, and an accuracy (linearity) of 0.1% of the full scale (Fig. 20). The data acquisition system that was used allowed displacements of 0.01 mm to be resolved. In addition to the joint meters a thermocouple and humidity transducer were installed in each system in order to track climatic changes. The monitoring program spanned a period of more than 30 months from September 1996 through January 1999. Data from each transducer were acquired and saved at 4 h intervals. Some of the acquired data are presented in Figs. 21 and 22.

Two distinct deformation modes are recognized: reversible, periodical, deformations (Fig. 21a), and a non-reversible, linear deformation (Figs. 21b and 22). The amplitude of the periodic mode in both systems rarely exceeds  $\pm 0.2$  mm from the preset zero values. These deformations have been interpreted as temperature controlled thermal expansion/contraction of the chalk. Based on the reversible nature and the relatively limited amplitude, this deformation pattern is considered non-destructive, although some studies [31] have concluded that cyclic thermal loading in weak rocks may lead to strength loss.

Destructive deformations in both systems are manifested by progressive, non-reversible, displacements of keyblocks (Figs. 21b and 22). The maximum non-reversible displacement was monitored by transducer SF4 (Fig. 21b)—1.5 mm over a period of 1 year. Similarly, Fig. 22 plots data acquired from three joint meters installed with the intent of monitoring the movement of a single keyblock in the roof of the northern system. Joint meter NF1 monitored block displacement in a direction perpendicular to the roof. Data collected from this transducer indicate continuous displacement of the keyblock into the cavern opening. In contrast joint meters NF2 and NF3 were positioned in order to monitor possible block displacement in directions tangential to the roof. Data acquired from these

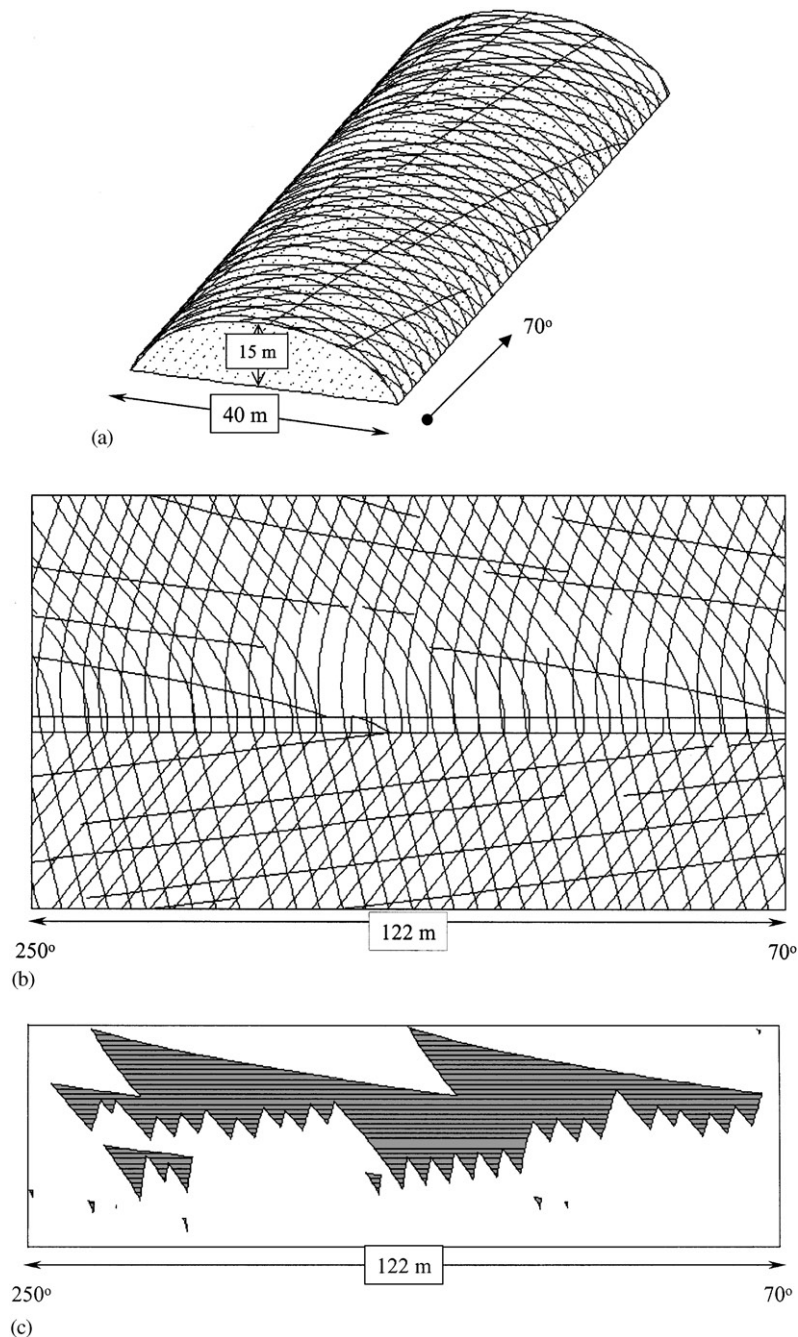


Fig. 18. Total removable keyblock area in the roof. Results of a single, proportional, joint spacing simulation ( $s_1 = 10$  m,  $s_2 = s_3 = 3.64$  m) using Shi and Goodman's unrolling algorithm [22]: (a) Joint trace map on tunnel walls as seen from outside the tunnel, (b) Unrolled joint trace map as seen from inside the tunnel, (c) Total removable keyblock area in the roof.

two transducers exhibit the non-destructive, reversible displacement mode.

Non-reversible keyblock displacements as monitored by transducers SF4 and NF1 (Figs. 21b and 22) may indicate possible rock yielding and crack growth at remote locations behind the cavern roof, due to the development of excessive tensile stresses as predicted by the numerical study. This complex yielding process, referred to above as 'mixed failure mode', may lead to

the relaxation of arching stresses, large keyblock displacements, and possibly global failure.

## 6. Summary and conclusions

- At Bet Guvrin National Park large-span caverns, excavated in a weak and discontinuous chalk, have been standing unsupported since the early Arabic

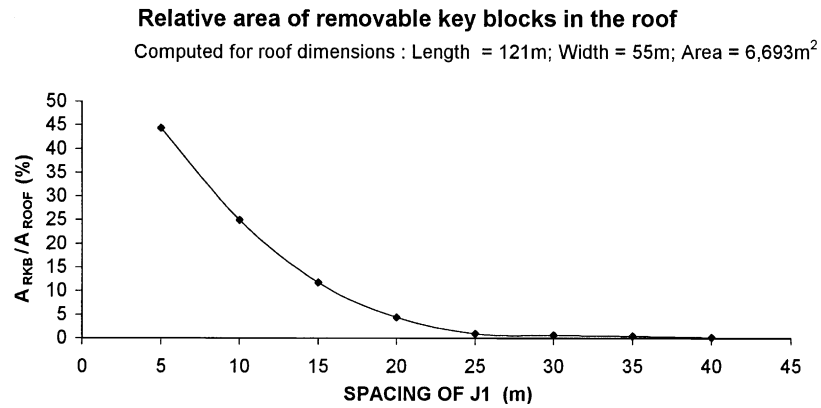


Fig. 19. Relationship between removable keyblock area in the roof and mean joint spacing obtained using joint trace and removable keyblock area simulation [22].

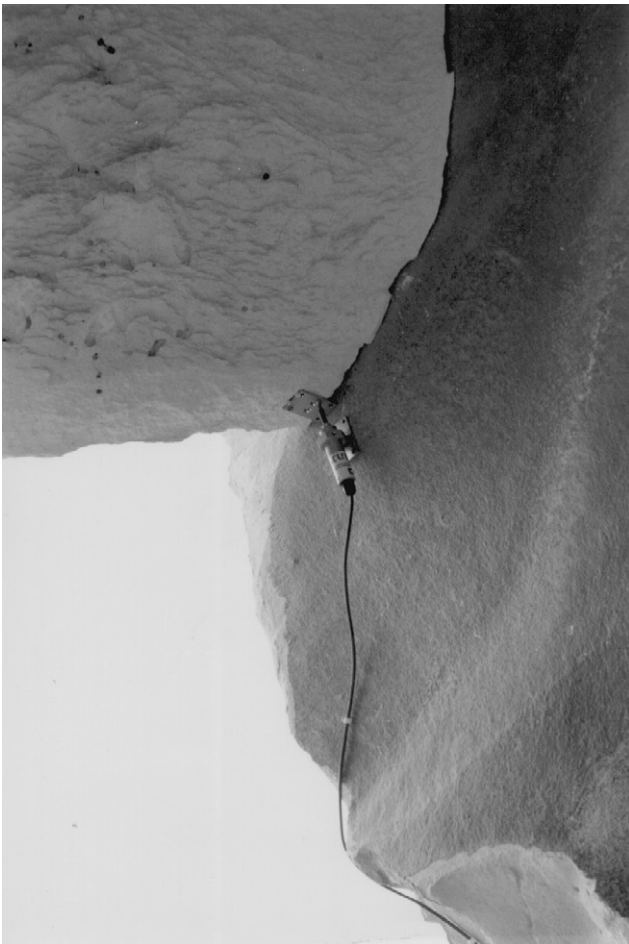


Fig. 20. An example of an LVDT type joint meter (Total transducer length—10 cm).

period, more than 1000 years ago. Typically the caverns exhibit free spans of 20–40 m and heights of 15–20 m.

- In the park there are evidences for different levels of cavern disintegration, from local keyblock failures, loss of pillars or common side-walls, and up to global collapse of entire systems.
- The rock mass is a weak and moderately jointed Eocene chalk of the Maresha formation.
- The strength of Maresha chalk is highly anisotropic with compressive strength normal and parallel to bedding of 6 and 9 MPa, respectively. Slight increases in water content drastically reduce the strength of the chalk but the degree of strength anisotropy (the peak strength ratio) remains the same over a wide range of water contents. The peak tensile strength in directions parallel to bedding under air dry condition is 1 MPa. The tensile strength is reduced by 60% as the water content is increased from 3% to 45%. These aspects of mechanical response have direct bearing on the assessment of the stability of the cavern openings.
- The results of *RMR* seem overly conservative, while the *Q* system returns realistic unsupported span predictions.
- Numerical stress analysis using *FLAC* shows that single caverns are safe against failure by crushing at the abutments or roof, even when a common sidewall separates between two adjacent caverns, as long as the sidewall thickness remains greater than 3 m. Common sidewalls of smaller thickness are incapable of sustaining the compressive stresses and will fail by crushing. Failure of common sidewalls will lead to the formation of huge caverns with a free span of 61 m. Such structures will fail due to tensile fracture nucleation and propagation at the roof. There are ample evidences for such failure processes in collapsed caverns at the park.
- Critical keyblock analysis shows that removable keyblock area in the roof increases with decreasing joint set spacing. With the mean joint set spacing at Bet Guvrin 45% of the roof area in the Southern system is expected to be covered with removable

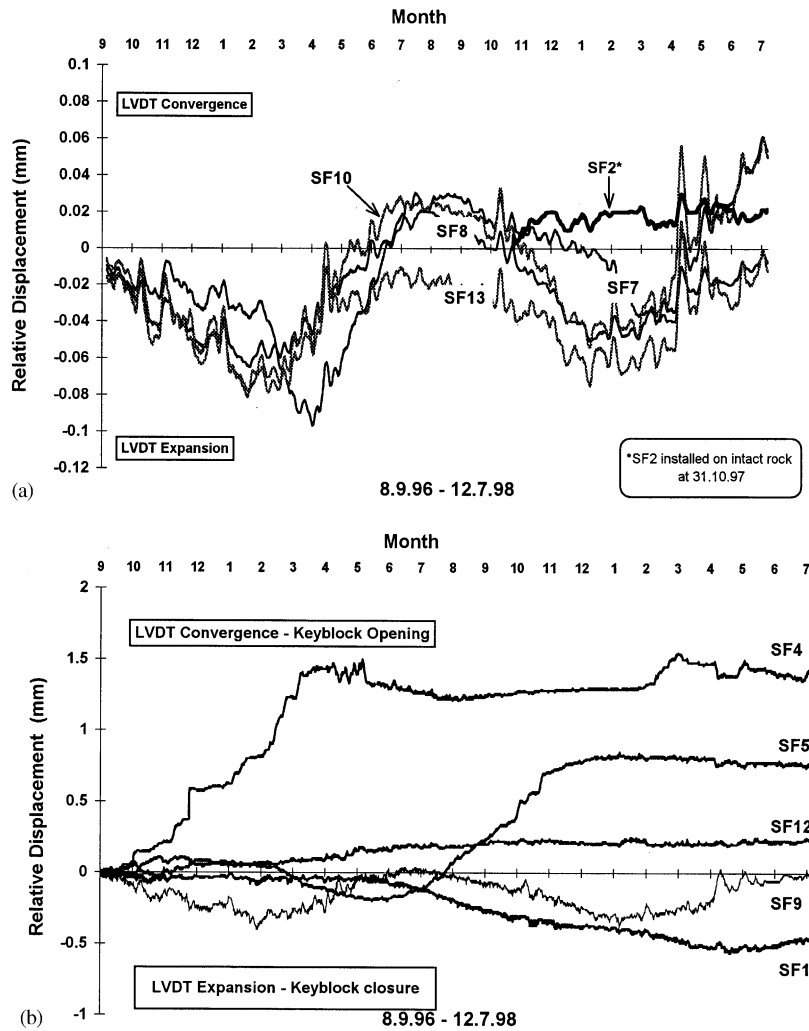


Fig. 21. Output of joint displacement monitoring program in the Southern system: (a) periodic displacement mode (heavy line—transducer SF2—shows output of dummy transducer which was installed on intact rock), (b) Linear displacement mode superposed on the characteristic periodic mode.

keyblocks. The blocks will remain in place as long as arching stresses are transmitted through the roof effectively. However, local failure processes in intact rock elements due to excessive stress concentrations may relax the arching process inducing excessive block displacements which may lead to global collapse. This failure mode is referred to here as a “mixed failure mode”.

- Our ability to predict the possibility of a “mixed failure mode” is based on simultaneous application of both continuous and discontinuous methods of analysis such as the numerical code FLAC, and the analytical keyblock theory.

- The results of a two year keyblock displacement monitoring program clearly suggests that excessive keyblock displacements are ongoing at present in two unsupported caverns with free spans of 30 and 40 m. While the rock mass can sustain the static loads, loss of keyblocks due to excessive displacements may endanger the stability of the entire structure due to the relaxation of the arching process at the roof.
- The results of the monitoring program together with the keyblock study and stress analyses can be utilized to map unstable zones in the caverns where “mixed failure mode” processes may be active at present. Efficient application of active support elements at

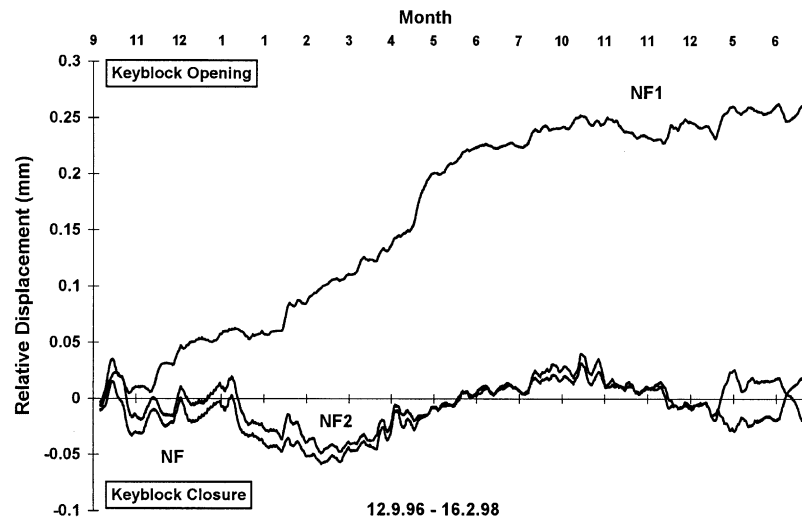


Fig. 22. The linear displacement mode as expressed by output from a keyblock in the roof of the Northern system (transducer NF1). Transducers NF2 and NF3 were installed outside the boundaries of the keyblock and show the characteristic periodic mode of the surrounding rock.

these locations will be necessary in order to ensure long-term stability.

### Acknowledgements

Israel Nature and Park Authority funded this research and their support is hereby acknowledged. The second author would like to acknowledge the support provided by the fund for the promotion of research at the Technion. Eng. Aharon Leviathan and Z. Margalit of the INPA are thanked for their professional support. Y. Blankstein and all the employees of the Bet Guvrin national park are thanked for their enthusiastic help in the field. We thank Professor J.A. Hudson for his interest in this work and for his instructive comments and suggestions. We also thank two anonymous reviewers for their constructive suggestions.

### References

- [1] Kloner A. Maresha, a guide. Israel Antiquities Authority, Jerusalem, 1996, 60pp [in Hebrew].
- [2] Talesnick ML, Hatzor YH, Tsesarsky M. The elastic deformability and strength of a high porosity, anisotropic, chalk. *Int J Rock Mech Min Sci* 2001;38(4):543–55.
- [3] Clough RW. Finite element method in plane stress analysis. *Proceedings of the Second ASCE Conference on Electronic Computation*, Pittsburgh, 1960.
- [4] Cundall PA, Board M. A microcomputer program for modeling large strain plasticity problems. In: Swoboda C, editor. *Numerical methods in geomechanics*. *Proceedings of the Sixth International Conference On numerical Methods in geomechanics*. Innsbruck, Rotterdam, Balkema, 1988. p. 2101–08.
- [5] Crouch SL, Strafield AM. *Boundary element method in solid mechanics*. London: George Allen and Unwin, 1983.
- [6] Goodman RE, Taylor RL, Brekke TL. A model for the mechanics of jointed rock. *J Soil Mech Found Div., Proceedings of the ASCE*, 94 SM3, 1968. p. 637–59.
- [7] Pariseau WG. Applications of finite element analysis to mining engineering. In: Hudson JA, editor. *Comprehensive Rock Engineering*, vol. 1(20). Oxford: Pergamon Press, 1993. p. 491–522.
- [8] Watson JO. An overview of the boundary element method. In: Hudson JA, editor. *Comprehensive rock engineering*, vol. 1(19), Oxford: Pergamon Press, 1993. p. 469–90.
- [9] Cundall PA. Numerical experiments on localization in frictional materials. *Ing-Arch* 1989;59:148–59.
- [10] Cundall PA. UDEC - A generalized distinct element program for modelling jointed rock, Final Technical Report on European Research Office (US Army Contract DAJA37-79-C-0548); NTIS order no. AD-A087 610/2, 1980.
- [11] Shi G-H. *Block system modeling by discontinuous deformation analysis*. Southampton, UK: Computational Mechanics Publications, 1993. p. 209.
- [12] Hart RD. An introduction to distinct element modelling for rock engineering. In: Hudson JA, editor. *Comprehensive rock engineering*, vol. 2 (20). Oxford: Pergamon Press, 1993. p. 491–522.
- [13] Shi G-H. Discontinuous deformation analysis: a new numerical model for the statics and dynamics of deformable block structures. *Eng Comput* 1992;9:157–68.
- [14] Yeung MR. Analysis of a three-hinged beam using DDA. In: Salami MR, Banks D, editors. *Proceedings of the first international forum on DDA and simulations of discontinuous media*. Albuquerque: TSI Press, 1996. p. 462–9.
- [15] Hatzor YH, Benary R. Stability of a laminated Voussoir beam: back analysis of a historic roof collapse using DDA. *Int J Rock Mech Min Sci* 1998;35(2):165–81.
- [16] Kim-Young, Amadei B, Pan E. Modeling the effect of water, excavation sequence and rock reinforcement with discontinuous deformation analysis. *Int J Rock Mech Min Sci* 1999;36(7): 949–70.
- [17] Goodman RE, Gen-Hua Shi. *Block theory and its application to rock engineering*. Englewood Cliffs, NJ: Prentice-Hall, Inc., 1985.

- [18] Hatzor Y, Goodman RE. Application of block theory and the critical key block concept to tunneling: two case histories. In: Myer LR, Cook NGW, Goodman RE, Tsang C, editors. Proceedings of ISRM conference on fractured and jointed rock masses. Rotterdam: Balkema, 1992. p. 663–70.
- [19] Hatzor Y, Goodman RE. Determination of the design block for tunnel supports in highly jointed rock. In: Hudson JA, editor. Comprehensive rock engineering, vol. 2: Analysis and design methods. Oxford: Pergamon Press, 1993. p. 263–92.
- [20] Tinucci JP, Funk CW. Optimizing excavation support using block theory to reorient tunnel direction. In: Amadei, Krantz, Scott, Smeallie, editors. Rock mechanics for industry. Rotterdam: Balkema, 1999. p. 551–7.
- [21] Hatzor Y. The block failure likelihood: a contribution to rock engineering in blocky rock masses. *Int J Rock Mech Min Sci* 1993;30(7):1591–7.
- [22] Shi, Gen-Hua, Goodman RE. The key blocks of unrolled joint traces in developed maps of tunnel walls. *Int J Numer Anal methods Geomech* 1989;13:131–58.
- [23] Tsesarsky M, Hatzor YH, Talesnick ML. The stability of Bet Guvrin caverns—integrated analysis in weak, anisotropic, and discontinuous chalk. *Isr J Earth Sci* 2000;49(2):81–102.
- [24] Barton NR, Lien R, Lunde J. Engineering classification of rock masses for the design of tunnel support. *Rock Mech* 1974;6:189–239.
- [25] Bieniawski ZT. Engineering classification of jointed rock masses. *Trans S Afr Inst Min Metall* 1976;74:335–44.
- [26] Itasca. FLAC—fast Lagrangian analysis of continua. Itasca Consulting Group. Minneapolis, Minnesota, 1995.
- [27] Hatzor YH. Validation of block theory using field case histories. Ph.D. Dissertation. Department of Civil Engineering, University of California, Berkeley, 1992.
- [28] Hatzor YH, Goodman RE. Three-dimensional back analysis of saturated rock slopes in discontinuous rock—a case study. *Geotechnique* 1997;47(4):817–39.
- [29] Mauldon M. Keyblock probabilities and size distributions: a first model for impersistent 2-D fractures. *Int J Rock Mech Min Sci* 1995;32(6):575–83.
- [30] Kuszmaul JS. Estimating keyblock sizes in underground excavations: accounting for joint spacing. *Int J Rock Mech Min Sci* 1999;36(2):217–32.
- [31] Inada Y, Kinoshita N, Ebisawa A, Shinji G. Strength and deformation characteristics of rocks after undergoing thermal hysteresis of high and low temperature. *Int J Rock Mech Min Sci Geomech Abstr* 1997;34:3–4, Paper No. 140.